

# Computational Model of Smoldering Combustion in Polyurethane Foam

S. Chatti<sup>†</sup>, C. Ghabi and A. Mhimid

Laboratory of Thermal and Energy Systems Studies, National Engineering School of Monastir, Monastir University, Monastir, Monastir, 5019, Tunisia

<sup>†</sup>Corresponding Author Email: Chatti\_saida@yahoo.com

(Received April 14, 2018; accepted July 23, 2018)

## ABSTRACT

Smoldering phenomenon can be described as a slow, low-temperature, flameless form of combustion, sustained by heterogeneous reactions with oxygen occurring at the surface of a condensed-phase fuel. In this work a computational study on the smoldering ignition and propagation in polyurethane foam is carried out. First, we investigated numerically the heat transfer and the fluid flow in porous media using the generalized lattice Boltzmann method (LBM). Our appropriate code is validated through the study of a thermal injected flow. LBM results are compared to analytical solutions and numerical results obtained using the Finite Difference Method. Second, the numerical model is extended to account for chemical reactions. We introduce the two-dimensional, transient, governing equations for smoldering combustion in a porous fuel. The model describes opposed and forward propagation according to appropriate assumptions. The kinetics model is based on a three-step mechanism. The temperature and char mass fraction profiles are studied at different cross-sections. Obtained results are compared to literature solutions. At the beginning, the important quantity of char is produced near the ignited boundary. To follow the phenomenon, the isotherms are presented at different instants. The results reproduce the features of the smoldering process and represent a significant step forward in smoldering combustion modeling.

**Keywords:** Chemical kinetics; Heat transfer; Lattice Boltzmann method; Porous media.

## NOMENCLATURE

$A$	frequency factor	$\alpha$	thermal diffusivity
$c_p$	specific heat capacity	$\Gamma_c, \Gamma_v, \Gamma_{h1}$	thermal, density, gas species
$c_0, c_1$	coefficients		relaxation time
$D_g$	gas diffusivity coefficients	$\delta t$	time step
$E$	activation energy	$\varepsilon$	porosity
$f$	density distribution function	$\rho$	char, gas, solid density
$g$	thermal distribution function	$\Delta H$	enthalpy
$h_1$	distribution function of gas mass	$\omega$	reaction rate
	fraction		
$i, j$	lattice indexes in the $x$ and $y$ direction	Subscript	
$K$	permeability	0	Initial
$k$	thermal conductivity	$th$	thermal
$n_{c1}, n_{c2}$		$a$	char oxidation or ash
$n_{o1}, n_{o2}$	stoichiometric coefficients	$c$	char
$n_{a3}, n_{g1}$		$g$	gas
$n_{g2}, n_{g3}$		$ox$	oxidation
$T$	temperature	$py$	pyrolysis
$u$	fluid velocity	$s$	solid or species
$Y$	species mas fraction	Superscript	
		$eq$	equilibrium

## 1. INTRODUCTION

Smoldering is a surface combustion reaction that propagates through a porous combustible material (Ohlemiller, 1986; Drysdale, 1987). The heat released in the reaction is characteristically low (Summerfield *et al.*, 1981). This phenomenon has been studied both computationally and experimentally. Ohlemiller (1986, 1995) provides two extensive review studies present in the literature. He proposed a 3-step and 3-species scheme, containing one pyrolysis and two oxidations, as the general scheme for the smoldering of fuel. Kashiwagi *et al.* (1992) estimated the kinetic parameters of this scheme for cellulose and polyurethane using thermogravimetric analysis (TGA) under nitrogen and air atmospheres. Rein *et al.* (2006) extended the Ohlemiller's scheme to five-step with four-species kinetics to study polyurethane foam. This extended scheme allows explaining the mechanism structure of a smoldering front in both forward and opposed propagation. Dodd *et al.* (2012) modeled two-dimensional smoldering in polyurethane foam using a two-dimensional numerical formulation that includes an eight-step kinetic mechanism. Many materials sustain smoldering combustion, including artificial fuels such as polyurethane foam or cellulosic insulation, and natural fuels such as coal or soils rich in organic matters. Huang *et al.* (2014) develop a one dimensional model of a reactive porous media to investigate smoldering combustion of natural fuels. The model is based on the open-source code Gpyro. Huang *et al.* (2014) used thermogravimetric data from the literature to propose and investigate a reaction scheme for the smoldering of peat. The scheme is based on five-step and five-species kinetics.

The understanding of the smoldering phenomenon necessitates the study of the heat transfer in porous media. One of most interesting and frequent situations is the flow in porous media. It has received considerable attention. This interest is explained by the variety of industrial applications mainly in aerodynamic engineering. Moreover, the control of the behavior of fluid flow and heat transfer in porous media remain crucial. It allows better optimization according to the desired objectives. A large number of studies were developed. Kaviany (1985) focused on the heat transfer and fluid flow in porous media bounded by two isothermal plates. The effect of thermodynamics parameters, like porosity and thermal conductivity, was discussed (Janzadeh, 2013).

The combustion problem is multidisciplinary. As mentioned, it involves a fluid mechanical process and heat transfer. This interaction limits our ability to handle such phenomena without numerical simulation. Thus, numerical techniques become essential for engineers and research scientists (Peters, 2000; Poinsoot *et al.*, 2001).

Recently, the lattice Boltzmann method (LBM) has emerged as an efficient alternative method for

numerical simulation (Li *et al.*, 2013). It is a mesoscopic technique that filled the gap between macroscopic and microscopic scales. The principle of LBM is the kinetic theory of fluid motion. It is derived from the Boltzmann transport equation. This method focuses on the behavior of a cluster of particles as a unit. In fact, the simulation with LBM consists of following the evolution of fluid particle in discretized space, speed and time (Tang, 2003). LBM received considerable attention due to many advantages: the convection operator of the equation is linear. It's adapted to parallel processes computing. Solving the Laplace equation is not necessary at each time step to satisfy the continuity equation. The Lattice Boltzmann method is used to model flow behavior in complex geometries thanks to its easy implementation under complex fluid-solid boundary conditions. In comparison with conventional CFD methods, the LBM uses a simple calculation procedure (Seta *et al.*, 2006; Guo *et al.*, 2002; Chatti *et al.*, 2015). The main advantage of this method is the simple implementation of boundary conditions. These advantages motivate the simulation of incompressible fluid flow in porous media.

In the present paper, we apply the LBM to study the smoldering combustion in polyurethane foam. The study implies, firstly, the investigation of heat and fluid flow in porous channel. We validate our code by the simulation of the thermal injected flow. The temperature and velocity profiles are presented for different Reynolds and Darcy numbers. The results are compared to numerical and analytical solution. The thermodynamics study is followed by a chemical investigation. The kinetic mechanism consists of three steps. The char mass fraction and the temperature profiles are presented at different cross-sections. The distribution of the temperature and the char mass fraction all over the medium describe the phenomenon evolution.

## 2. NUMERICAL METHOD: LATTICE BOLTZMANN METHOD

The lattice Boltzmann method is an efficient tool for complex phenomena simulation. The LBM has inherent advantages as parallel implementation, aptitude to treat complex geometries and easy expression of boundary conditions.

In this paper, a novel lattice BGK (Bhatnagar, Gross and Krook) approach for reactive flow is proposed. It is strictly a pure lattice Boltzmann model. The momentum, temperature, and gas species conservation equations are solved using only the lattice Boltzmann method.

This approach is based on the double-distribution-function model proposed by Shan *et al.* (1997). Its main feature is the simulation of velocity, temperature, and species fields by two sets of distribution functions.

The algorithm describes a simple process of hopping from one point to the next. The standard lattice Boltzmann method are retained due to its better numerical stability.

### a. Flow Fields

For incompressible flow, the evolution equation of the density is as follows (Seta 2009, 2010):

$$f(x + \delta t c_i, t + dt)_i + f(x, t)_i = \frac{f(x, t)_i - f(x, t)_i^{eq}}{\Gamma_\nu} + \delta t F_i \quad (1)$$

The discrete velocities of the D2Q9 model (Fig. 1) are:

$$\begin{cases} c_0 = 0 \\ c_i = c \left( \cos\left((i-1)\frac{\pi}{2}\right), \sin\left((i-1)\frac{\pi}{2}\right) \right) \text{ for } i = 1, 4 \\ c_i = c \left( \cos\left((i-1)\frac{\pi}{2} + \frac{\pi}{4}\right), \sin\left((i-1)\frac{\pi}{2} + \frac{\pi}{4}\right) \right) \\ \text{for } i = 5, 8 \end{cases} \quad (2)$$

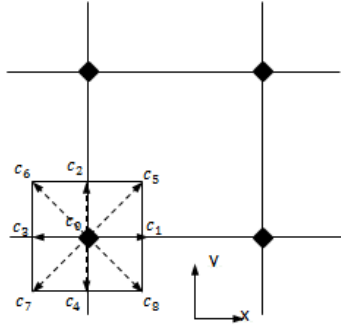


Fig. 1. D2Q9 Model.

The weights are:

$$\begin{cases} \omega_0 = \frac{4}{9} \\ \omega_i = \frac{1}{9} \text{ for } i = 1, 4 \\ \omega_i = \frac{1}{36} \text{ for } i = 5, 8 \end{cases}$$

The equilibrium distribution function is given by (Seta 2009, 2010):

$$f_i^{eq} = \omega_i \rho \left[ 1 + \frac{3c_i \cdot u}{c^2} + \frac{9(c_i \cdot u)^2}{2\varepsilon^4} - \frac{3u \cdot u}{2\varepsilon c^2} \right] \quad (3)$$

The total external body force is expressed by (Seta 2009, 2010):

$$F_i = \omega_i \rho \left( 1 - \frac{1}{2\Gamma_\nu} \right) \left[ \frac{3c_i \cdot F}{c^2} + \frac{9(uF \otimes c_i c_i)}{\varepsilon c^4} - \frac{3u \cdot F}{\varepsilon c^2} \right] \quad (4)$$

The macroscopic density and velocity are expressed as follows (Seta 2009, 2010):

$$\rho(x, t) = \sum_i f(x, t)_i, \quad u(x, t) = \sum_i \frac{c_i f(x, t)_i}{\rho} + \frac{F \delta t}{2} \quad (5)$$

The kinetic viscosity is expressed in the lattice unit using the following relation:

$$\nu = \frac{2\Gamma_\nu - 1}{6} c^2 \delta t \quad (6)$$

### b. Temperature Fields

The evolution equation of the temperature is as follows (Chiavazzo *et al.*, 2009):

$$g(x + \delta t c_i, t + dt)_i + g(x, t)_i = \frac{g(x, t)_i - g(x, t)_i^{eq}}{\Gamma_c} + \omega_i \delta t Q_i \quad (7)$$

$Q_i$  is a source term due to chemical reactions. In LB calculation,  $Q_i$  is given by the similarity in non-dimensional equations of temperature.

For D2Q9, the equilibrium distribution functions are:

$$\begin{cases} g_0^{eq} = \frac{2\rho T}{3} \frac{u \cdot u}{c^2} \\ g_i^{eq} = \frac{\rho T}{9} \left[ \frac{3}{2} + \frac{3c_i \cdot u}{c^2} + \frac{9(c_i \cdot u)^2}{c^4} - \frac{3u \cdot u}{2c^2} \right] \\ \text{for } i = 1, 4 \\ g_i^{eq} = \frac{\rho T}{36} \left[ 3 + \frac{6c_i \cdot u}{c^2} + \frac{9(c_i \cdot u)^2}{c^4} - \frac{3u \cdot u}{2c^2} \right] \\ \text{for } i = 5, 8 \end{cases} \quad (8)$$

$c$  refers to the lattice spacing ( $c = 1$ ).

The thermal diffusivity is expressed as follows (Chiavazzo *et al.*, 2011):

$$D_{th} = \frac{2\Gamma_c - 1}{6} c^2 \delta t \quad (9)$$

The macroscopic temperature,  $T$ , is obtained by:

$$T(x, t) = \sum_i g(x, t)_i \quad (10)$$

### c. Species Fields

The evolution equation of gas mass fraction is as follows (Yamamoto *et al.*, 2002):

$$h_1(x + \delta t c_i, t + dt)_i + h_1(x, t)_i = \frac{h_1(x, t)_i - h_1(x, t)_i^{eq}}{\Gamma_{h1}} + \omega_i \delta t Q_c \quad (11)$$

$Q_c$  is a source term due to chemical reactions. In LB calculation,  $Q_c$  is given by the similarity in non-dimensional equations of species fields. For the oxygen, this term is given by:

$$Q_c = \frac{1}{\varepsilon} \frac{\rho_{s0}}{\rho_{g0}} \left( n_{o1} \omega_{ox}^* + n_{o3} \omega_a^* \right)$$

For D2Q9, the equilibrium distribution functions are:

$$\left\{ \begin{array}{l} h_{i0}^{eq} = \frac{2\rho_g Y_g u \cdot u}{3 c^2} \\ h_{i1}^{eq} = \frac{\rho_g Y_g}{9} \left[ \frac{3}{2} + \frac{3 c_i \cdot u}{2 c^2} + \frac{9 (c_i \cdot u)^2}{2 c^4} - \frac{3 u \cdot u}{2 c^2} \right] \\ \text{for } i = 1,4 \\ h_{i1}^{eq} = \frac{\rho_g Y_g}{36} \left[ 3 + \frac{6 c_i \cdot u}{c^2} + \frac{9 (c_i \cdot u)^2}{2 c^4} - \frac{3 u \cdot u}{2 c^2} \right] \\ \text{for } i = 5,8 \end{array} \right. \quad (12)$$

The  $S$  specie diffusivity is:

$$D_{gs} = \frac{2\Gamma_{h1}-1}{6} c^2 \delta t \quad (13)$$

The reaction rate of the  $R$  reaction is as follows (Chiavazzo *et al.*, 2009):

$$(\omega_R)_{LBM} = \frac{\omega_R L_c}{\rho_{ph} \mu_0} \left( \frac{\rho_0 \mu_0}{L_c} \right)_{LBM} \quad (14)$$

$\rho_{ph}$  is the density in physical unit.

The macroscopic gas mass fraction,  $Y_g$ , are obtained in terms of the distribution function by:

$$Y_g = \sum_i h_{i1}(x, t) \quad (15)$$

#### d. Numerical Validation

The code validation was ensured by the study of the thermal injected flow. The situation is a channel traversed by incompressible and laminar flow. The cold top wall ( $T(x, H) = T_c$ ) is moving with a constant velocity  $u_0$ , while hot ( $T(x, 0) = T_h$ ) bottom wall is fixed. A fluid is injected from the bottom with constant velocity  $v_0$  and withdrawn from the top (Seta *et al.*, 2006) (Fig. 2).

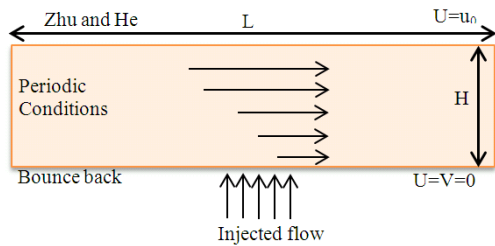


**Fig. 2. Problem configuration.**

The Reynolds number is defined by  $Re = \frac{v_0 H}{\nu}$ .

The Darcy, Prandtl and Rayleigh numbers are

$$Da = \frac{K}{H^2}, Pr = \frac{\nu}{\chi} \text{ and } Ra = \frac{g_0 \beta \Delta T H^2}{\nu \chi}.$$

The numerical simulation was done with a mesh of  $80 \times 80$ . The Prandtl and Rayleigh numbers are

respectively 0.71 and 100. When the porosity is equal to 1.0 and the Darcy number is 0.0, the analytical solutions of velocity and temperature, in steady state, are as follows:

$$\begin{aligned} u &= v_0 \left( \frac{\exp\left(\frac{Re^* y}{H}\right) - 1}{\exp(Re) - 1} \right), T = T_c + \\ \Delta T * &\left( \frac{\exp\left(\frac{Re^* Pr^* y}{H}\right) - 1}{\exp(Re^* Pr) - 1} \right) \end{aligned} \quad (16)$$

The difference between hot and cold plates is  $\Delta T = T_h - T_c$ .

For the upper wall, the velocity is known. Several approaches can be adopted. In our study, we consider Zou and He method based on mass and momentum conservation to determine unknown distribution functions (Chatti *et al.*, 2016). The periodic conditions express the velocities on the right and left sides. They are given by:

$$f(k, 1, j)_{k=1,5,8} = f(k, n, j)_{k=3,6,7} \quad (17)$$

The bounce back is applied on the bottom wall. It is given by the following equation:

$$f(k, i, 1)_{k=2,5,6} = f(-k, i, 1)_{k=2,5,6} \quad (18)$$

The Dirichlet conditions handle the temperature behavior on the boundary. For the bottom wall, they are expressed as follows:

$$g(k, i, 1)_{k=2,5,6} = T_h (\omega_k + \omega_{k+2}) - g(k, i, 1)_{k=4,7,8} \quad (19)$$

At the outlet, the open boundary conditions are used.

$$g(k, n, j)_{k=3,6,7} = 2g(k, n-1, j)_{k=3,6,7} - g(k, n-2, j)_{k=3,6,7} \quad (20)$$

The root mean square error (RMSE) was calculated between analytical solutions and presents results. It is expressed as follows:

$$E_{moy} = \sqrt{\frac{\sum_1^m (V_{LBM} - V_s)^2}{m}} \quad (21)$$

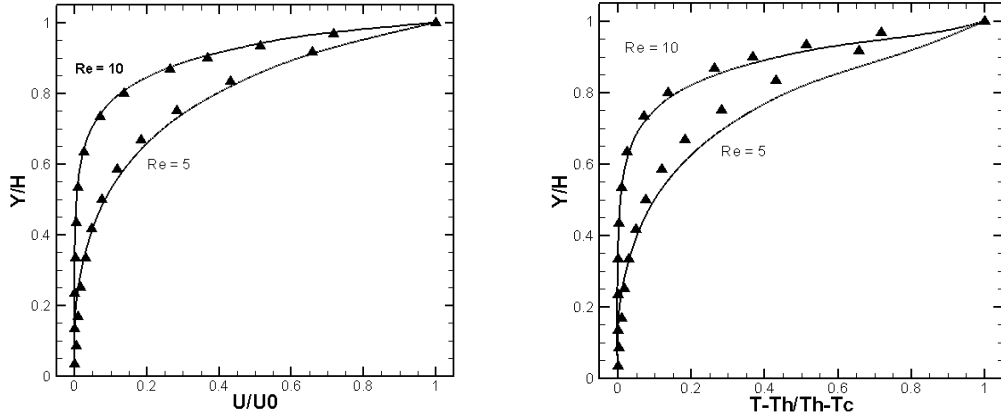
Where  $V_s$  refers to analytical solution and  $V_{LBM}$  to LBM result. The sum includes  $m$  values.

Table 1 expresses the velocity and temperature root mean square error for different Reynolds numbers.

Figure 3 shows the velocity and temperature profiles along the channel. We superposed analytic solution to numerical velocity profile in the perpendicular plane to the axis of the flow at a distance equal to  $L/2$  from the channel inlet.

**Table 1 Velocity Root Mean square error**

Reynolds number	Velocity RMSE between analytic and LBM results	Temperature RMSE between analytic and LBM results
5	0.065240545	0.077383477
10	0.022681331	0.018389702



**Fig. 3. Velocity and temperature profiles at different Reynolds numbers. The solid lines are the LBM results and the symbols are analytical values.**

An excellent agreement was observed between the two types of solutions.

### 3. HEAT TRANSFER IN POROUS MEDIA

#### a. Mathematical Equations

In porous media the governing equations are given in the representative elementary volume approach (REV). We adopt the Boussinesq approximation. Indeed, the incompressible fluid flow and heat transfer are described by the following equations (Guo *et al.*, 2002; Seta *et al.*, 2006; Shokouhmand *et al.*, 2011; Haghshenas *et al.*, 2010):

Continuity equation

$$\nabla u = 0 \quad (22)$$

Momentum equation

$$\frac{\partial u}{\partial t} + (u \cdot \nabla) \left( \frac{u}{\varepsilon} \right) = -\frac{1}{\rho_g} \nabla(\varepsilon p) + \nu_e \nabla^2 u + F \quad (23)$$

Energy equation

$$\sigma \frac{\partial T}{\partial t} + \nabla \cdot (uT) = \alpha \nabla^2 T \quad (24)$$

The relation between  $\sigma$  and  $\alpha$  is  $\alpha = \sigma c_s^2 (\Gamma_c - 0.5)$ . The bulk average pressure  $p$  is expressed by:

$$p = \frac{\rho_g c^2}{3\varepsilon} \quad (25)$$

The effective viscosity  $\nu_e$  is assumed to be equal to

the viscosity  $\nu$ , and  $F$  represents the total external body force containing porous media resistance.  $G$  is an external force. The general expression is:

$$F = -\frac{\varepsilon \nu}{K} u - \frac{\varepsilon F_E}{\sqrt{K}} |u| u + \varepsilon G \quad (26)$$

The geometric function is  $F_E = \frac{1.75}{\sqrt{150\varepsilon^3}}$ . This

expression leads to the generalized lattice Boltzmann equation. The forcing term is given by (Seta *et al.*, 2006). To avoid the non-linearity, we define a temporal velocity  $v$  by the following relation (Seta *et al.*, 2006; Guo *et al.*, 2002; Chatti *et al.*, 2016).

$$u = \frac{v}{c_0 + \sqrt{c_0^2 + c_1 |v|}} \quad (27)$$

In order to highlight our choice to the generalized lattice Boltzmann equation, we treated the previous problem in a porous channel using the finite difference method (FDM). A parametric study was achieved in a steady state. Figure 4 illustrates a comparison between the LBM and the FDM. It concerns the velocity profiles for different Reynolds and Darcy number. Through this figure we noted an excellent agreement between the two approaches. This agreement allows us to confirm the validity of our code and its ability to simulate fluid flow in porous media. Comparing the time required to obtain a converged solution, for the same conditions, we note a significant time lag. Consequently, we adopt the generalized lattice Boltzmann method (GLBE). This choice ensures an important gain in simulation time.

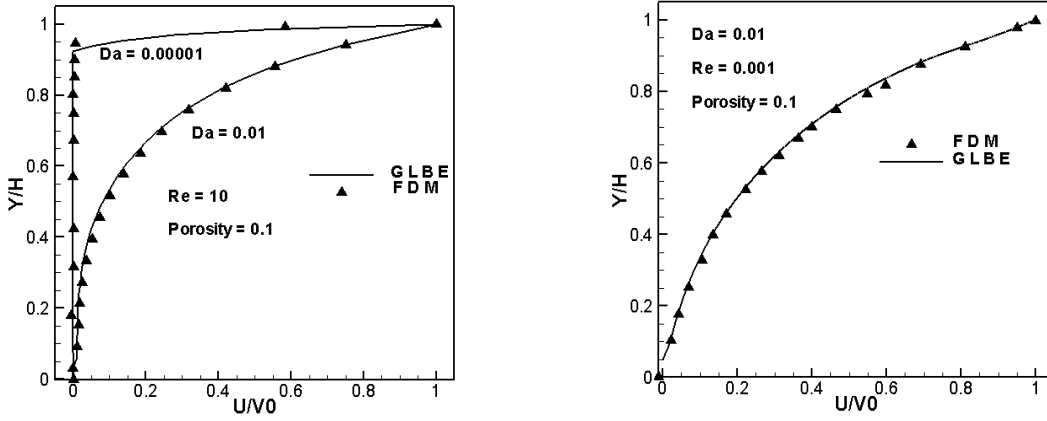


Fig. 4. Velocity profile for different Darcy and Reynolds numbers.

#### 4. SMOLDERING IN POLYURETHANE FOAM

##### a. Physical Problem

The physical problem is illustrated in Fig. 5. It consists of a fixed bed of polyurethane foam with a length and width of 15 cm. Initially, all the foam fuel is unreacted. Air is forced to flow into the left face of the porous medium. The combustion process is initiated by applying a high temperature or a high heat flux at the front during a period of time until we obtain the self-sustainment of the reaction. The reaction zone propagates from the left to the right side of the medium.

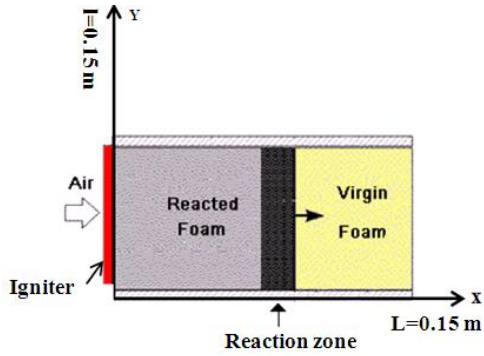


Fig. 5. Forward smoldering of fixed bed of foam.

##### b. Heat and Mass Transfer Coefficients

It is convenient to define heat and mass transfer coefficients in terms of dimensionless numbers. The Nusselt, Reynolds and Prandtl numbers are correlated by the Wakao and Kagueli relations (Leach *et al.*, 2000):

$$Nu = 2 + 1.1 \left( Re^2 Pr \right)^{\frac{1}{3}}$$

Where the Reynolds and Prandtl numbers are defined as:

$$Re = \frac{u \varepsilon d_p}{\nu} \text{ and } Pr = \frac{\nu}{\alpha}$$

The specific surface of the exchange between the solid and the fluid is related to the porosity and the pore diameter by (Leach *et al.*, 2000):

$$s = \frac{4(1-\varepsilon)}{d_p} \quad (28)$$

We assume that the char and the ash have identical physical properties. The solid phase' characteristics are defined using the char and ash mass fraction. The effect of radiation is modeled in the optically thick limit; using the Rosseland approximation (Ghabi *et al.*, 2007a). We introduce radiation conductivity  $k_{rad}$ , the total thermal conductivity of the solid  $k_s$  is:

$$\begin{cases} k_{rad} = \frac{16\sigma d_p T_s^3}{3} \\ k_s = (Y_c + Y_a)k_{c0} + (1 - Y_c - Y_a)k_{s0} \end{cases} \quad (29)$$

The solid density and heat capacity are defined as follows (Lautenberger *et al.*, 2009; Dodd *et al.*, 2009):

$$\begin{cases} \rho_s = (Y_c + Y_a)\rho_{c0} + (1 - Y_c - Y_a)\rho_{s0} \\ c_{ps} = (Y_c + Y_a)c_{pc0} + (1 - Y_c - Y_a)c_{ps0} \end{cases} \quad (30)$$

The gas and the total heat flux are calculated through the following expression (Dosanjh *et al.*, 1987):

$$\begin{aligned} M_g &= \varepsilon \rho_g u \\ M_t &= M_g + M_s \end{aligned} \quad (31)$$

The Lewis, the Schmidt and the Peclet numbers are given by:

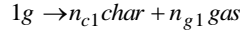
$$Le = \frac{\alpha}{D_g} = \frac{k_g}{\rho_g c_{pg} D_g}, Sc = \frac{\nu}{D_g}, Pe = \frac{L_c u_0}{D_g}$$

##### c. Kinetic Model

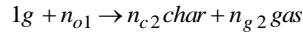
The chemical reactivity is modeled by a three-step mechanism. Indeed, the fuel decomposes through endothermic pyrolysis giving gaseous products and solid char. The fuel undergoes oxidation. The

second step is the char oxidation; it is a highly exothermic reaction in which the char is converted to gaseous products and ash. The mechanism is reported by Ghabi *et al.* (2007 a, b). It is also studied by Rein *et al.* (2005, 2006). For simplification, the gaseous species (thermal pyrolyzate and products) are considered as a single species “gas”. The mechanism is summarized as follows:

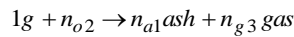
The fuel pyrolysis:



The fuel oxidation:



The char oxidation:



The reaction rates are of Arrhenius type. They depend on the solid fuel and the oxygen concentration. Their mathematical expressions are (Leach *et al.*, 2000):

**Thermal oxidation**

$$\omega_{ox} = (1 - Y_c - Y_a)^f \rho_s A_{ox} (Y_{o2})^m \exp\left(-\frac{E_{ox}}{RT}\right) \quad (32)$$

**Pyrolysis**

$$\omega_{py} = (1 - Y_c - Y_a)^g \rho_s A_{py} \exp\left(-\frac{E_{py}}{RT}\right) \quad (33)$$

**Char oxidation**

$$\omega_a = Y_c \rho_c A_a (Y_{o2})^h \exp\left(-\frac{E_a}{RT}\right) \quad (34)$$

The coefficients *f*, *g*, *h*, and *m* represent the orders of the above chemical reactions.

The kinetics parameters (pre-exponential factors, activation energies, reaction orders, and stoichiometry coefficients) are summarized in Table 2 (Ghabi *et al.*, 2007 a, b; Dodd *et al.*, 2009).

**d. Mathematical Formalism**

**i. Assumption**

The mathematical model treats the two-dimensional time-dependent conservation equations for the forward smoldering combustion. It is based on the following assumptions:

The gaseous species have identical diffusion coefficients.

The gases released by pyrolysis and oxidation leave the medium before reacting.

The gas diffusion is modeled by Fick's law.

The gas velocity at the surface is zero. The general form of Darcy law is applied.

The gas is incompressible and the properties of the fluid and solid phases are constants.

The reactions didn't cause the shrinkage of volume. The heat and the oxygen diffuse from the solid surface to the bulk gas.

The porous medium and the flowing gas are homogeneous and isotropic.

The porous matrix is rigid.

The porous medium absolute permeability is constant.

The gravitational effects are neglected.

The chemical reactions occur at the surface of the fuel and depend on the oxygen concentration.

The local thermal equilibrium is established between solid and gas phases.

**Table 2 Kinetics parameters for the oxidation and pyrolysis of polyurethane foam**

Variables	Values
$A_{ox}, A_{py}, A_a$	$5.69 \cdot 10^{11}, 2 \cdot 10^{17}, 5 \cdot 10^8 \text{ s}^{-1}$
$E_{ox}, E_{py}, E_a$	159.88, 220.215, 159.88 K
$C_{p_{s0}}, C_{p_{c0}}, C_{p_{g0}}$	$1.7 \text{ kJkg}^{-1}\text{K}^{-1}, 1.1 \text{ kJkg}^{-1}\text{K}^{-1}, 1.03 \text{ kJkg}^{-1}\text{K}^{-1}$
$D_0$	$4.53 \cdot 10^{-5} \text{ m}^2 \text{ s}^{-1}$
$d_p$	$5 \cdot 10^{-5} \text{ m}$
$h, h_w$	$0.7 \text{ Wm}^{-1}\text{k}^{-1}, 0.07 \text{ Wm}^{-1}\text{k}^{-1}$
$n_{c1}, n_{c2}, n_{o1}, n_{o2}, n_{g1}, n_{g2}, n_{g3}, n_{a1}$	0.21, 0.24, 0.41, 1.65, 0.03, 1.2, 0.76, 2.62
$R$	$8.31 \text{ Jmol}^{-1}\text{K}^{-1}$
$T_0$	300 K
$u_0$	$0.0053 \text{ ms}^{-1}$
$\varepsilon$	0.975
$k_{g0}, k_{s0}, k_{c0}$	$2.5 \cdot 10^{-2}, 6.3 \cdot 10^{-2}, 4.2 \cdot 10^{-2} \text{ Wm}^{-1}\text{K}^{-1}$
$\rho_{c0}, \rho_{g0}, \rho_{s0}$	$10 \text{ kgm}^{-3}, 1.04 \text{ kgm}^{-3}, 26.5 \text{ kgm}^{-3}$
$\Delta H_{ox}, \Delta H_{py}, \Delta H_a$	-5700 J/g, 500 J/g, -25000 J/g

**ii. Governing Equations**

The mathematical model is based on the following conservation equations:

**Solid phase species conservation:**

$$\frac{\partial(\rho_s Y_c)}{\partial t} = \frac{1}{(1-\varepsilon)} (n_{c2}\omega_{ox} + n_{c1}\omega_{py} - \omega_a) \quad (35)$$

$$\frac{\partial(\rho_s Y_a)}{\partial t} = \frac{1}{(1-\varepsilon)} (n_{a1}\omega_a) \quad (36)$$

**Gas phase species conservation (Oxygen conservation)**

$$\frac{\partial(\rho_g Y_{o2})}{\partial t} + \nabla(\rho_g Y_{o2} u) = D_g \nabla^2(\rho_g Y_{o2}) - \frac{1}{\varepsilon}(n_{o1}\omega_{ox} + n_{o2}\omega_a) \quad (37)$$

#### Gas phase mass conservation

$$\frac{\partial \rho_g}{\partial t} + \nabla \cdot (\rho_g u) = \frac{1}{\varepsilon} \left( \begin{array}{l} (n_{g2} - n_{o1})\omega_{ox} + n_{g1}\omega_{py} \\ + (n_{g3} - n_{o2})\omega_a \end{array} \right) \quad (38)$$

#### Solid phase mass conservation

$$\frac{\partial \rho_s}{\partial t} = -\frac{1}{(1-\varepsilon)} \left( \begin{array}{l} (n_{g2} - n_{o1})\omega_{ox} \\ + n_{g1}\omega_{py} \\ + (n_{g2} - n_{o2})\omega_a \end{array} \right) \quad (39)$$

#### Momentum conservation

$$\frac{\partial u}{\partial t} + (u \cdot \nabla) \left( \frac{u}{\varepsilon} \right) = -\frac{1}{\rho_g} \nabla(\varepsilon p) + \nu \nabla^2 u - \frac{\varepsilon \nu}{K} u - \frac{\varepsilon F_E}{\sqrt{K}} |u| u \quad (40)$$

#### Energy conservation

$$\left( \rho_g \varepsilon c_{p_g} + (1-\varepsilon) \rho_g c_{p_g} \right) \frac{\partial T}{\partial t} + \rho_g c_{p_g} \nabla(\varepsilon u T) = \nabla \cdot \left( \begin{array}{l} (k_{seff} + k_{geff}) \nabla T \\ - (\omega_{ox} \Delta H_{ox} + \omega_{py} \Delta H_{py}) \\ + \omega_a \Delta H_a \end{array} \right) \quad (41)$$

### iii. Initial and Boundary Conditions

The left side is sustained at constant temperature until the smoldering reaction get started (i.e. the foam's maximum temperature reached, and the combustion reaction goes away from the igniter).

On the right boundary (outlet) an established regime is considered and the gradients are equal to zero.

At  $t = 0$  s the entire fuel is unreacted, the temperature is constant and equal to the ambient temperature:

$$\begin{cases} T = 300 K \\ Y_{o2} = 0.22 \\ Y_c = Y_a = 0.0, Y_s = 1.0 \end{cases} \quad (42)$$

The upper and lower walls are impermeable. For velocity and species mass fraction, we consider:

$$(\nabla \varphi)_{y=0,L} = 0.0 \varphi = u, Y_s \quad (43)$$

For the thermal Boundary, the following relations are adopted:

$$(\nabla T)_{y=0,L} = \frac{h_w}{k_{seff}} (T - T_{ext})$$

$$(\nabla T)_{x=0} = \frac{h}{k_{seff}} (T - T_{ext}) \quad (44)$$

On the outlet we apply the following condition for the temperature and the species mass fraction:

$$(\nabla \varphi)_{x=L} = 0.0 \varphi = T, Y_s \quad (45)$$

### iv. Dimensionless Equations

The governing equations are given in terms of dimensionless numbers and parameters. It is required for numerical simulation. We define the following variables:

$$L_c = \frac{(1-\varepsilon)k_{s0} + \varepsilon k_{g0}}{((1-\varepsilon)c_{ps0} + \varepsilon c_{pg0})M_{ti}}, t_c = \frac{L_c}{u_0}$$

$$\theta = \frac{T - T_0}{T_{max} - T_0}, x^* = \frac{x}{L_c}, y^* = \frac{y}{L_c}, u^* = \frac{u}{u_0}, t^* = \frac{tu_0}{L_c}$$

$$p^* = \frac{p}{\rho_g \theta u_0^2}, \omega_{ox}^* = \frac{L_c \omega_{ox}}{\rho_s \theta u_0}, \omega_{py}^* = \frac{L_c \omega_{py}}{\rho_s \theta u_0}$$

$$\omega_{ox}^* = \frac{L_c \omega_{ox}}{\rho_s \theta u_0}$$

#### Dimensionless solid species conservation

$$\frac{\partial Y_c}{\partial t^*} = \frac{1}{(1-\varepsilon)} (n_{c2}\omega_{ox}^* + n_{c1}\omega_{py}^* - \omega_a^*) \quad (46)$$

$$\frac{\partial Y_a}{\partial t^*} = \frac{1}{(1-\varepsilon)} (n_{a1}\omega_a^*) \quad (47)$$

#### Dimensionless oxygen conservation

$$\frac{\partial Y_{o2}}{\partial t^*} + \nabla^* (Y_{o2} u^*) = \frac{1}{Pe} \nabla^{*2} Y_{o2} \quad (48)$$

$$-\frac{\rho_{s0}}{\varepsilon \rho_{g0}} (n_{o1}\omega_{ox}^* + n_{o2}\omega_a^*)$$

#### Dimensionless gas phase mass conservation

$$\nabla^* \cdot u^* = \frac{\rho_{s0}}{\varepsilon \rho_{g0}} \left( \begin{array}{l} (n_{g2} - n_{o1})\omega_{ox}^* + n_{g1}\omega_{py}^* \\ + (n_{g3} - n_{o2})\omega_a^* \end{array} \right) \quad (49)$$

#### Dimensionless momentum conservation

$$\frac{\partial u^*}{\partial t^*} + (u^* \cdot \nabla^*) \left( \frac{u^*}{\varepsilon} \right) = -\nabla^* (\varepsilon p^*) + \frac{1}{Re} \nabla^{*2} u^* \quad (50)$$

$$-\frac{\varepsilon}{Da^* Re} u^* - \frac{\varepsilon F_E}{\sqrt{K}} |u^*| u^*$$

#### Dimensionless solid energy conservation

$$R_{keff} = \frac{(1-\varepsilon)k_s + k_{rad}}{k_g}, R_c = \frac{\rho_s c_{ps}}{\rho_g c_{pg}}$$

$$R_{H_{ox}} = \frac{\Delta H_{ox}}{c_{ps}(T_{max} - T_0)}, R_{H_{py}} = \frac{\Delta H_{py}}{c_{ps}(T_{max} - T_0)}$$

$$R_{H_a} = \frac{\Delta H_a}{c_{ps}(T_{max} - T_0)}$$

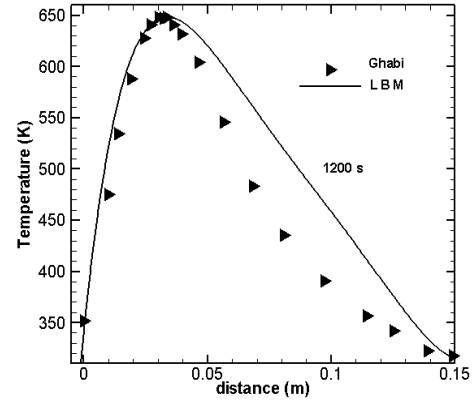
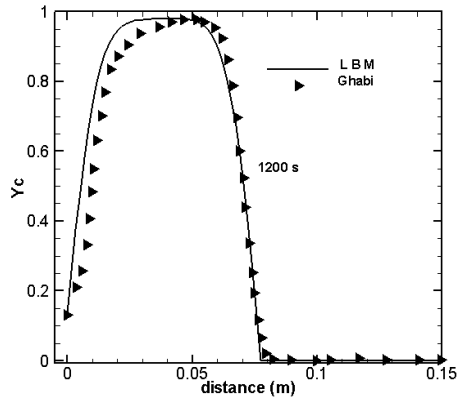


Fig. 6. Char mass fraction and temperature profiles.

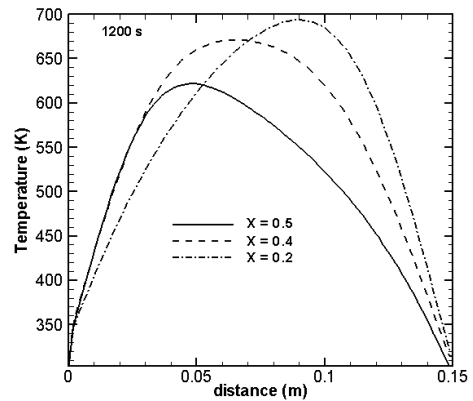
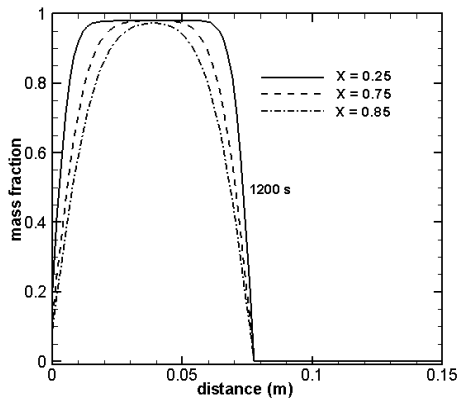


Fig. 7. Char mass fraction and temperature at different cross sections.

$$\frac{\partial \theta}{\partial t^*} + \frac{1}{(\varepsilon + (1-\varepsilon)R_c)} \rho_g c_{p_g} \nabla^* (\varepsilon u^* \theta) = \frac{R_{keff}}{(\varepsilon + (1-\varepsilon)R_c)} \frac{1}{Pr^* Re} \nabla^{*2} \theta - \frac{R_c}{(\varepsilon + (1-\varepsilon)R_c)} \left( \frac{R_{H_{ox}} \omega_{ox}^* + R_{H_{py}} \omega_{py}^*}{+ R_{H_a} \omega_a} \right) - \frac{1}{(\varepsilon + (1-\varepsilon)R_c)} \frac{T_0}{(T_{max} - T_0)} \frac{\rho_{s,0}}{\varepsilon \rho_{g,0}} \left( \frac{(n_{g2} - n_{o1}) \omega_{ox}^* + n_{g1} \omega_{py}^*}{+(n_{g3} - n_{o2}) \omega_a^*} \right) \quad (51)$$

### e. Simulation Results

To evaluate the validity of our model, the situation presented in Fig. 5 is simulated. It is a frequent test that was previously studied for example by Ghabi *et al.*, (2007) and Rein *et al.*, (2005).

In this paper, we define appropriate assumptions. For the flow, the temperature and the species mass fractions, bounce back boundary conditions are applied.

Figure 6 shows the present and Ghabi's results for the temperature and char mass fraction at 1200 s. These results are obtained using our appropriate numerical code based on the lattice Boltzmann method.

Table 3 illustrates the relative error between the

actual results and the Ghabi's solution.

Table 3 Temperature and char mass fraction relative error

Temperature relative error (Ghabi/LBM)	Mass fraction relative error (Ghabi/ LBM)
0.045119	0.0372

The noted difference between LBM results and Ghabi's solution is explained by the assumptions adopted during the simulation. Our model is based on local thermal equilibrium. In contrary, Ghabi's work is based on a two-temperature model (the computational domain is out of thermal equilibrium). Another reason for this difference is the term of exchange between the solid matrix and the fluids. In the present model we neglect this term. However, Ghabi's model accounts for the solid-fluid exchanges. Moreover, the difference originates from the dissimilarity of the studied configuration and consequently the applied boundary conditions. Indeed, the present results are obtained for a rectangular geometry while those of Ghabi are obtained for a cylindrical geometry.

We are interested in the phenomenon evolution inside the polyurethane foam. For a specific time, the temperature and the char profiles are presented at different sections of the medium. Through the following figure, we note that at the beginning (t = 1200 s) the important quantity of char is produced

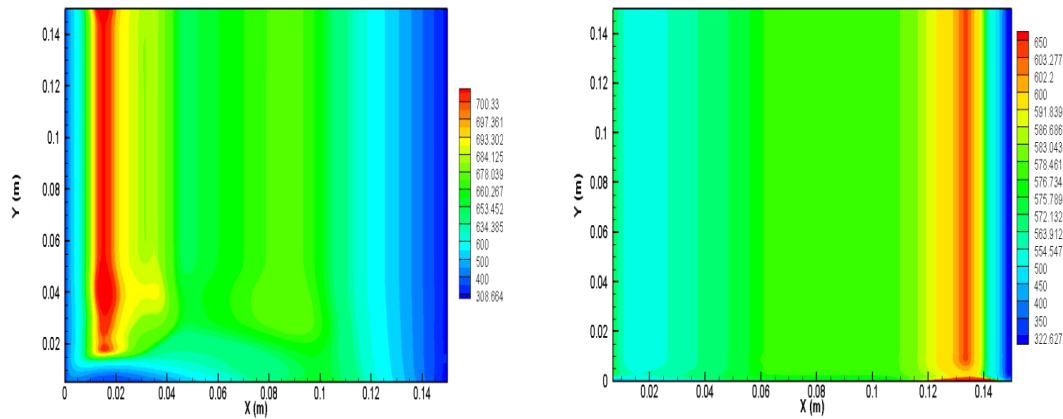


Fig. 8. Isotherms at  $t = 1150(s)$  (left) and  $t = 1450(s)$  (right).

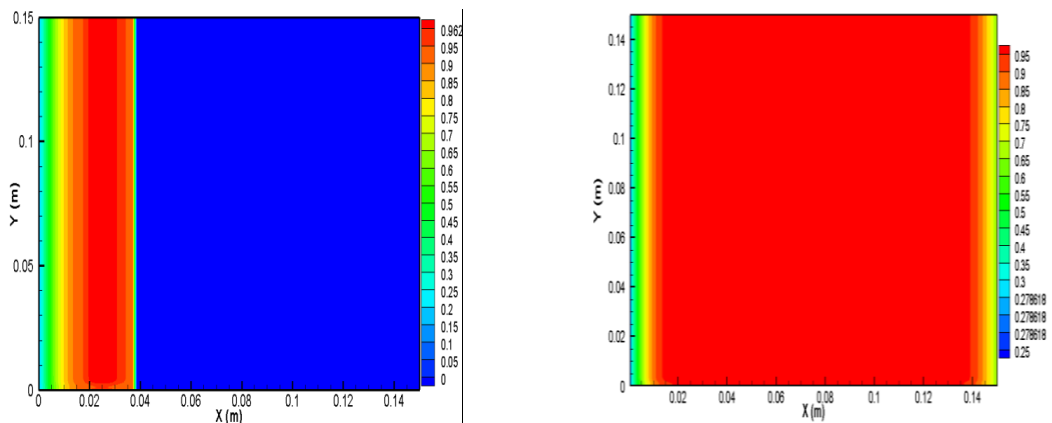


Fig. 9. Char mass fraction at  $t = 1150(s)$  (left) and  $t = 1450(s)$  (right).

near the inlet face (left face). By entrance inside the medium, this quantity is less intense. Initially, due to the incoming cold air, a very small amount of char is formed near the inlet face. The production of the char is more important on the sections close to the ignition face. For the same instant, the maximum temperature is important inside the foam (preheated zone) the fuel undergoes exothermic pyrolysis.

The Fig. 8 shows the distribution of the temperature in the medium at the beginning and the end of the reaction. It presents the isotherms at 1150 s and 1450 s.

Through this figure, we observe a curvature in the reaction zone near the wall side. A hot zone appears near the reaction zone and reduces near the wall. This can be explained by the heat dissipation from the combustion zone to the wall. The gross zone is characterized by low temperature. The heat released by the exothermic oxidation is transferred ahead of the reaction zone by conduction, convection and radiation. It preheats the unreacted fuel. The increase of the temperature is the origin of smoldering sustainability and mechanism continuity. It allows the reaction propagation through the foam. A portion of this heat is lost through the side wall. This figure carries out the propagation of the reaction.

Figure 9 shows char mass fraction distribution at different moments. At the beginning, due to the incoming cold air, a small quantity of char is formed near the ignition side. The non-converted zone of polyurethane appears near the air inlet and particularly close to the side wall. Due to the smoldering forward propagation, fuel is converted into char. So, the char mass fraction attains the unit.

The unreacted zone ( $Y_c < 0.1$ ) appears near the wall side. The heat deficiency explains the presence of this zone. At the end of the combustion reaction, the original polyurethane is not totally transformed into char.

## 5. CONCLUSION

The smoldering combustion is slow flameless combustion. The phenomenon is heterogeneous and occurs in the interior or on the surface of the porous fuel. It encompasses numerous fields such as chemical reactions and heat transfer.

It is important to study, firstly, the heat transfer and fluid flow in porous media. Indeed, we validate our appropriate code, based on the generalized lattice Boltzmann method, using benchmark case. Then, we treated the thermal injected flow in the porous channel using the finite difference method (FDM). A comparison between the two approaches allowed

concluding the validity of our code and the preference of LBM due to its rapidity.

The modulation of smoldering phenomenon needs the application of particular assumptions. We adopted the mechanism based on three kinetic reactions. It is governed by the conservation equations. The resolution of these equations is not always available. The numerical simulation is an efficient tool. This is the first time that the smoldering combustion of polyurethane foam is simulated using the generalized lattice Boltzmann. The temperature and the char mass fraction are compared to literature works. Then, the results are presented for different cross-sections. Initially, a small quantity of char is formed. This quantity is essentially located near the ignited side. The maximum of temperature increases progressively inside the medium. The distribution of temperature highlights the propagation of phenomenon inside the medium.

Future work will focus on the effect of oxygen concentration on smoldering combustion and species mass fraction evolution all over medium.

## REFERENCES

- Chatti, S., C. Ghabi and A. Mhimid (2015). Effect of obstacle presence for heat transfer in porous Channel. *Lecture Notes in Mechanical engineering 2015*, 823-832.
- Chatti, S., C. Ghabi and A. Mhimid (2016). Fluid flow and heat transfer in porous media and post heated obstacle: lattice Boltzmann simulation. *International Journal of Heat and Technology 34*, 377-385.
- Chiavazzo, E., I. V. Karlin, A. N. Gorban and K. Boulouchos (2009). Combustion simulation via lattice Boltzmann and reduced chemical kinetics. *Journal of Statistical Mechanics: Theory and Experiment 2009*, 1-22.
- Chiavazzo, E., I. V. Karlin, A. N. Gorban and K. Boulouchos (2011). Efficient simulations of detailed combustion fields via the lattice Boltzmann method. *International Journal of Numerical Methods for Heat and Fluid Flow 21*, 494-517.
- Dodd, A. B., C. Lautenberger and A. C. Fernandez-Pello (2009). Numerical examination of two-dimensional smolder structure in polyurethane foam. *Proceedings of the Combustion Institute 32*, 2497-2504.
- Dodd, A. B., C. Lautenberger and C. Fernandez-Pello (2012). Computational modeling of smolder combustion and spontaneous transition to flaming. *Combustion and Flame 159*, 448-46.
- Dosanji, S. Sudip, P. J. Pagni and A. C. Fernandez-Pello (1987). Forced Co-current Smoldering Combustion. *Combustion and Flame 68*, 131-142.
- Drysdale, D. (1987). *An Introduction to Fire Dynamics*. New York, John Wiley and Sons 256, 1-576.
- Ghabi C., H. Benticha and M. Sassi (2007a). Computational modelling and simulation of forward-smoldering of porous media in a fixed bed. *Progress in Computational Fluid Dynamics 7*, 283-293.
- Ghabi C., H. Benticha and M. Sassi (2007b). Parametric study of the heat transfer coefficient in bi-dimensional smoldering simulation. *Thermal Science 11*, 95-112.
- Guo, Z. and T. S. Zhao (2002). Lattice Boltzmann model for incompressible flows through porous media. *Physical review 66*, 036304-1-036304-9.
- Haghshenas, A., M. Rafati Nasr and M. H. Rahimian (2010). Numerical simulation of natural convection in an open-ended square cavity filled with porous medium by lattice Boltzmann method. *International Communications in Heat and Mass Transfer 37*, 1513-1519.
- Huang, X. and G. Rein (2014). Smoldering combustion of peat in wildfires: Inverse modeling of the drying and the thermal and oxidative decomposition kinetics. *Combustion and Flame 161*, 1633-1644.
- Janzadeh, N. and M. A. Delavar (2013). Using lattice Boltzmann method to investigate the effects of porous media on heat transfer from solid block inside a channel. *Transport Phenomena in Nano and Micro Scales 1*, 117-123.
- Kashiwagi, T. and H. Nambu (1992). Global kinetic constants for thermal oxidative degradation of a cellulosic paper. *Combustion and Flame 88*, 345-368.
- Kaviany, M. (1985). Laminar flow through a porous channel bounded by isothermal parallel plate. *International Journal of Heat and Mass Transfer 28*, 851-858.
- Lautenberger, C. and C. Fernandez-Pello (2009). Generalized pyrolysis model for combustible solids. *Fire Safety Journal 44*, 819-839.
- Leach, S. V., G. Rein, J. L. Ellzey and O. A. Ezekoye and J. L. Torero (2000). Kinetic and fuel property effects on forward smoldering combustion. *Combustion and Flame 120*, 346-358.
- Li, L., R. Mei and J. F. Klausner (2013). Boundary conditions for thermal lattice Boltzmann equation method. *Journal of Computational Physics 237*, 366-395.
- Ohlemiller, T. J. (1995). *The SFPE Handbook of Fire Protection Engineering*, 3rd ed., NFPA, Quincy, MA.
- Ohlemiller, T. J. (1986). Modeling of smoldering combustion propagation. *Progress in Energy Combustion Science 11*, 277-310.

- Peters, N. (2000). *Turbulent combustion*. Cambridge University Press, Cambridge.
- Poinsot, T. and D. Veynante (2001). Theoretical and numerical combustion, R.T. Edwards Inc., Philadelphia.
- Rein, G., A. B. Ilan, A. C. Fernandez-Pello, J. L. Ellzey, J. L. Torero and D. L. Urban (2005). Modeling of one-dimensional smoldering of polyurethane in microgravity conditions. *Proceedings of the Combustion Institute* 30, 2327–2334.
- Rein, G., C. Lautenberger, A. C. Fernandez-Pello, J. L. Torero and D. L. Urban (2006). Application of genetic algorithms and thermogravimetry to determine the kinetics of polyurethane foam in smoldering combustion. *Combustion and Flame* 146, 95–108.
- Seta, T. (2009). Lattice Boltzmann Method for fluid flows in anisotropic porous media with Brinkman equation. *Journal of Fluid Science and Technology* 4, 116-127.
- Seta, T. (2010). Lattice Boltzmann method for natural convection in anisotropic porous media. *Journal of Fluid Science and Technology* 5, 585-602.
- Seta, T., E. Takegoshi, K. Kitano and K. Okui (2006). Thermal lattice Boltzmann model for incompressible flows through porous media. *Journal of Thermal Science and Technology* 1, 90-100.
- Shan, X. (1997). Simulation of Rayleigh-Bernard convection using a lattice Boltzmann method. *Physical Review E* 55, 2780–2788.
- Shokouhmand, H., F. Jam and M. R. Salimpour (2011). The effect of porous insert position on the enhanced heat transfer in partially filled channels. *International Communications in Heat and Mass Transfer* 38, 1162-1167.
- Summerfield, M. and N. Mesina (1981). Smoldering combustion in porous fuels. *Prog. Astronaut.* 73, 129-194.
- Tang, G. H., W. Q. Tao and Y. L. He (2003). Simulation of fluid flow and heat transfer in a plane channel using the lattice Boltzmann method. *International journal of modern physics B* 17, 183-187.
- Yamamoto, K., X. He and G. D. Doolen (2002). Simulation of Combustion Field with Lattice Boltzmann Method. *Journal of Statistical Physics* 107, 367 – 383.